Hindawi
International Journal of Antennas and Propagation
Volume 2022, Article ID 6157022, 7 pages
https://doi.org/10.1155/2022/6157022

Research Article

Composite Scattering from a PEC Object above Two-Layered Rough Soil Surfaces Based on an Efficient Bi-Iterative Model

Ke Li, Lixin Guo, and Juan Li

School of Physics, Xidian University, Xi'an, China

Correspondence should be addressed to Ke Li; xidian_keli@163.com and Lixin Guo; lxguo@xidian.edu.cn

Received 24 May 2022; Revised 16 October 2022; Accepted 28 November 2022; Published 31 December 2022

Academic Editor: Giuseppe Castaldi

In the study, an efficient bi-iterative physical optics (PO) electromagnetic model is used to analyze the composite scattering from a PEC object above two-layered rough soil surfaces for the first time. The PO method is applied to calculate the direct scattered fields from the object and the upper layer rough surface and to deal with the mutual coupling effect between the object and the two-layered rough surfaces. During the mutual coupling process, a bi-iterative strategy is considered to solve the coupling interaction between the object and the upper rough surface and the coupling interaction between the upper and lower rough surfaces. We assume a 2-D scattering problem. The result is validated by comparing it with that obtained from the conventional method of moments (MoM). Comparison results from different object types show that the scattered curves calculated using the proposed method resemble the ones obtained from MoM. The comparison of computer resources also shows the efficiency of our method. Meanwhile, the normalized radar cross-section of the composite model is analyzed under different parameters.

1. Introduction

Actual natural backgrounds, such as the Earth's surface (forest, snow, desert, and ocean scenarios), and all kinds of artificial material surfaces, can be regarded as random rough surface models. Scattering of electromagnetic (EM) waves from rough surfaces has been studied for over half a century since the 1950s [1, 2]. The natural surfaces are modeled as single layered rough surfaces in the early days. However, many scenarios mentioned above consist of two-layered or multilayer rough surfaces. Radar remote sensing from the Earth holds great realistic significance, such as retrieval of soil properties and finding camouflaged targets above the land. Thus, most related applications concerning surveillance to the soil, target tracking, and navigation communication in complex backgrounds are explored. For example, L-band soil moisture active and passive missions are identified as a priority for NASA's Science Mission Directorate [3], L-band Soil Moisture and Ocean Salinity Missions are conducted by the European Space Agency [4], and an experiment of autonomous vessel tracking in simulated rough sea conditions is implemented by Villanova University [5].

Apart from the experiments, theoretical simulation methods are also used to examine rough surfaces. Because of the flexibility and high precision, numerical methods and their improved methods are always used to calculate the composite scattering from the object and rough surfaces. For example, the method of moments (MoM) [6], the finite difference time domain (FDTD) method [7], and the finite element method (FEM) [8]. However, the numerical methods consume a lot of computer resources, which limit their scope of application. Notably, proper combinations, such as the combination of approximate method with numerical method can result in high computational efficiency while maintaining the desirable precision. Examples are the hybrid analytic-numerical algorithm combining the Kirchhoff approximation (KA) with the method of moments (MoM) [9], the method combining KA with the hybrid finite element-boundary integral [10], and the hybrid method combining physical optics (PO) with PO [11, 12]. However, these works are either ineffective or not applied further on most actual scenarios, such as forest covered with vegetation, land covered with snow, and even same visual soil with different moisture contents in layer depth. To date, some

methods are used to calculate the properties of layered rough surfaces, such as iterative physical optics (IPO) model [13], physical optics approximation (POA) algorithm [14], or used to analyze the polarimetric scattering from two-layered random rough surfaces with and without buried objects, such as the KA model [15] and the steepest descent fast multipole method (SDFMM) [16]. However, research on composite scattering from the object above the layered rough surface is limited, except the work complemented by Wang and Li [17, 18]. This scarcity is due to the intricate coupling interaction between the object and the layered rough surface that complicates the problem further.

The aforementioned problems motivate the investigation on scattering from the object above multilayered soil rough surfaces. In this study, the soil is modeled as a two-layered rough surface with a Gaussian spectrum [17] by using the Monte Carlo method, and each layer has different soil moisture contents. The objects are cylinder and square cylinder. A bi-iterative PO is adopted to solve the coupling interaction between the object and the upper rough surface and the coupling interaction between the upper and lower rough surfaces. The normalized radar cross-section (NRCS) of the composite model is validated by comparing the results with those obtained from the conventional MoM. In this study, all fields and currents are assumed to have a time-harmonic dependence in the form $e^{-i\omega t}$, which is suppressed in this study.

2. Theoretical Formulations of the Bi-Iterative Model

The bi-iterative model in this study is an extension of our work in [12]: a PEC object partially buried in a rough sea surface. Specifically, we developed it further on and expanded the method to a more complicated model than before with an object above layered rough surfaces. The complication is the single layer rough surface is extended to a two-layered rough surface. Thus, the coupling scattering is complicated further and the scattering mechanism should be explored between the two-layered rough surfaces. Furthermore, the numerical calculation of the rough surface often accounts for the most amount of the computation in the problem of composite scattering of the object and rough surfaces, so the attempt to develop a method to measure the scattering effectively, accelerate the calculation, and analyze the coupling scattering mechanisms of the object and rough surfaces (especially for the two-layer rough surfaces) is a valuable task. The detailed solution is expressed as follows:

The geometry of the problem of interest is shown in Figure 1. $\widehat{\mathbf{k}}_i$ is the incident wave unit vector, and $\widehat{\mathbf{k}}_s$ is the scattered wave unit vector. θ_i is the incident angle, θ_s is the scattered angle. Meanwhile, we assume that the simulated rough surfaces have large radii of the curvature to enable the use of the PO method.

The soil surface is modeled as a two-layered rough surface, and the profile of the two-layered rough surface divides the entire space into three spaces. They are labeled as Ω_0, Ω_1, and Ω_2. S_o denotes the object in space Ω_0, S_1 denotes the upper layer surface with a profile $\varsigma_1(x)$, and S_2 denotes the lower layer with a profile $\varsigma_2(x)$; S_o, S_1, and S_2 are used as

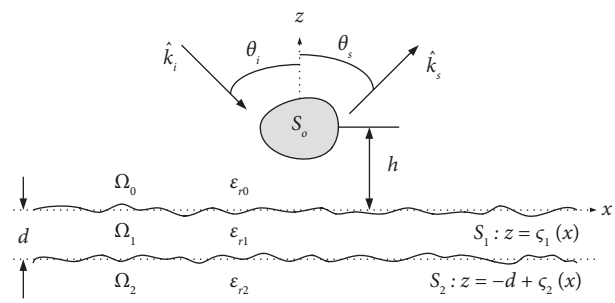

Figure 1: The geometry of a PEC object above a two-layered rough surface.

subscripts in the subsequent current variables. S_1 and S_2 are generated by the Monte Carlo method. We assume that S_1 and S_2 are uncorrelated. h is the altitude of the object, and d is the average thickness of the S_1 layer. h and d must be sufficiently large to avoid the profile spatial overlap. Ω_0, Ω_1, and Ω_2 are characterized by relative permittivities ε_{r0}, ε_{r1}, and ε_{r2}. For the model in our study, $\varepsilon_{r0} = 1$.

2.1. The Direct Scattering from Space Ω_0. We use horizontal (HH) polarization as an example. The incident wave $\mathbf{E}^{\text{inc}}(\mathbf{r}) = \widehat{\mathbf{y}}\phi^{\text{inc}}(\mathbf{r})$ excites equivalent induced currents on the surfaces located in space Ω_0 with the assumption that S_o and S_1 are independent, where $\phi^{\text{inc}}(\mathbf{r})$ is Thorsos tapered plane wave [19]. The currents on S_o and S_1 are represented as $\mathbf{J}^1_{s_o}$ and $\mathbf{J}^1_{s_1}, \mathbf{M}^1_{s_1}$. The superscript number represents the order number of currents, and they are the same for subsequent variables. The first-order equivalent currents are obtained by the PO method and represented as

$$\mathbf{J}^1_{s_o}(\mathbf{r}) = 2\widehat{\mathbf{n}}_o \times \mathbf{H}^{\text{inc}}(\mathbf{r})\,(\mathbf{r} \in S_o), \tag{1}$$

$$\mathbf{J}^1_{s_1}(\mathbf{r}) = \left(1 - R^H_{01}\right)\widehat{\mathbf{n}}_1 \times \mathbf{H}^{\text{inc}}(\mathbf{r})\,(\mathbf{r} \in S_1), \tag{2a}$$

$$\mathbf{M}^1_{s_1}(\mathbf{r}) = \left(1 + R^H_{01}\right)\mathbf{E}^{\text{inc}}(\mathbf{r}) \times \widehat{\mathbf{n}}_1\,(\mathbf{r} \in S_1), \tag{2b}$$

where $\widehat{\mathbf{n}}_o$ is the surface normal vector to S_o, $\widehat{\mathbf{n}}_1$ is the upper surface normal vector to S_1, and the reflection coefficient R^H_{01} is expressed as follows:

$$R^H_{01} = \frac{\sqrt{\varepsilon_{r0}}\cos\theta_l - \sqrt{\varepsilon_{r1} - \varepsilon_{r0}\sin^2\theta_l}}{\sqrt{\varepsilon_{r0}}\cos\theta_l + \sqrt{\varepsilon_{r1} - \varepsilon_{r0}\sin^2\theta_l}}\left(\cos\theta_l = -\widehat{\mathbf{k}}_i \cdot \widehat{\mathbf{n}}_1\right). \tag{3}$$

We provide a detailed explanation to (3) because it will be used frequently in the following analysis with a regular pattern. R^H_{01} is the reflection coefficient on the boundaries of Ω_0 and Ω_1, and subscripts "0" and "1" are related to the parameters in Ω_0 and Ω_1, respectively. "01" indicates that the wave is incident in Ω_0 and the refractive in Ω_1. θ_l is the local incident angle on the boundary and is determined by the incident wave and normal vectors of boundary at the incident side.

2.2. The Mutual Coupling Strategy among the Boundaries. We assume the $(n-1)$ th-order equivalent induced currents $\mathbf{J}^{n-1}_{s_o}$ and $\mathbf{J}^{n-1}_{s_1}, \mathbf{M}^{n-1}_{s_1}$ scatter fields in space Ω_0. We also

introduce the equivalent currents on the lower surface of S_1 and denote them as $\mathbf{J}_{s_1'}^{n-1}, \mathbf{M}_{s_1'}^{n-1}$. $\mathbf{J}_{s_1'}^{n-1}, \mathbf{M}_{s_1'}^{n-1}$ and $\mathbf{J}_{s_2}^{n-1}, \mathbf{M}_{s_2}^{n-1}$ scatter fields in space Ω_1'. From the boundary conditions, we can reason out that

$$\mathbf{J}_{s_1'}^{n-1} = -\mathbf{J}_{s_1}^{n-1}; \mathbf{M}_{s_1'}^{n-1} = -\mathbf{M}_{s_1}^{n-1} (n \geq 2). \tag{4}$$

An overview of the coupling iterative procedure is described as follows: (a) the scattered fields excited by $\mathbf{J}_{s_1}^{n-1}$ and $\mathbf{M}_{s_1}^{n-1}$ travel to S_o, and the n th-order currents $\mathbf{J}_{s_o}^{n}$ on S_o are obtained; (b) the scattered fields excited by $\mathbf{J}_{s_o}^{n-1}$ travel to S_1, and the n th-order currents $\mathbf{J}_{s_{1-1}}^{n}$ and $\mathbf{M}_{s_{1-1}}^{n}$ on the upper surface of S_1 are obtained; (c) the scattered fields excited by $\mathbf{J}_{s_1'}^{n-1}$ and $\mathbf{M}_{s_1'}^{n-1}$ travel to S_2, and the n th-order currents $\mathbf{J}_{s_2}^{n}$ and $\mathbf{M}_{s_2}^{n}$ on S_2 are obtained; (d) the scattered fields excited by $\mathbf{J}_{s_2}^{n-1}$ and $\mathbf{M}_{s_2}^{n-1}$ travel to S_1, and the n th-order currents $\mathbf{J}_{s_{1-2}}^{n}$ and $\mathbf{M}_{s_{1-2}}^{n}$ on the lower surface of S_1 are obtained. The n th equivalent currents are obtained by the PO method. The detailed coupling procedure is shown in Figure 2.

In Figure 2, the primary and secondary currents are marked in black and blue, respectively. The solid line with an arrow represents the coupling relation described as (a)–(d). The dashed line with an arrow represents the direction of the current updating, which indicates that the secondary currents will replace the last currents and can be used to calculate the next order currents. The newly induced currents on the upper surface of S_1 are expressed as follows:

$$\mathbf{J}_{s_1}^{n} = \mathbf{J}_{s_{1-1}}^{n} - \mathbf{J}_{s_{1-2}}^{n}; \mathbf{M}_{s_1}^{n} = \mathbf{M}_{s_{1-1}}^{n} - \mathbf{M}_{s_{1-2}}^{n} (n \geq 2). \tag{5}$$

Then, equivalent currents on the lower surface of S_1 can be obtained from (4). The currents on the upper and lower surfaces will iterate in Ω_0 and Ω_1, respectively. This model is the so-called bi-iterative model. The initial currents are the directly induced currents excited by the tapered plane wave in (1) and (2). Notably, $\mathbf{J}_{s_2}^{1} = 0$ and $\mathbf{M}_{s_2}^{1} = 0$.

The expression of the induced equivalent currents on the surfaces can be written as follows:

$$\mathbf{J}_{s_o}^{n}(\mathbf{r}) = 2\hat{\mathbf{n}}_o \times \mathbf{L}_1\left(\mathbf{J}_{s_1}^{n-1}, \mathbf{M}_{s_1}^{n-1}\right)(\mathbf{r} \in S_o), \tag{6}$$

$$\mathbf{J}_{s_{1-1}}^{n}(\mathbf{r}) = \left(1 - R_{01}^{H}\right)\hat{\mathbf{n}}_1 \times \mathbf{L}_1\left(\mathbf{J}_{s_o}^{n-1}\right)(\mathbf{r} \in S_1), \tag{7a}$$

$$\mathbf{M}_{s_{1-1}}^{n}(\mathbf{r}) = \left(1 + R_{01}^{H}\right)\mathbf{K}_1\left(\mathbf{J}_{s_o}^{n-1}\right) \times \hat{\mathbf{n}}_1(\mathbf{r} \in S_1), \tag{7b}$$

$$\mathbf{J}_{s_2}^{n}(\mathbf{r}) = \left(1 - R_{12}^{H}\right)\hat{\mathbf{n}}_2 \times \mathbf{L}_2\left(\mathbf{J}_{s_1'}^{n-1}, \mathbf{M}_{s_1'}^{n-1}\right)(\mathbf{r} \in S_2), \tag{8a}$$

$$\mathbf{M}_{s_2}^{n}(\mathbf{r}) = \left(1 + R_{12}^{H}\right)\mathbf{K}_2\left(\mathbf{J}_{s_1'}^{n-1}, \mathbf{M}_{s_1'}^{n-1}\right) \times \hat{\mathbf{n}}_2(\mathbf{r} \in S_2), \tag{8b}$$

$$\mathbf{J}_{s_{1-2}}^{n}(\mathbf{r}) = \left(1 - R_{10}^{H}\right)\hat{\mathbf{n}}_1' \times \mathbf{L}_2\left(\mathbf{J}_{s_2}^{n-1}, \mathbf{M}_{s_2}^{n-1}\right)(\mathbf{r} \in S_1), \tag{9a}$$

$$\mathbf{M}_{s_{1-2}}^{n}(\mathbf{r}) = \left(1 + R_{10}^{H}\right)\mathbf{K}_2\left(\mathbf{J}_{s_2}^{n-1}, \mathbf{M}_{s_2}^{n-1}\right) \times \hat{\mathbf{n}}_1'(\mathbf{r} \in S_1). \tag{9b}$$

Equations (6)–(9) correspond to (a)–(d), respectively. The definition of reflection coefficients R_{01}^{H}, R_{12}^{H}, and R_{10}^{H} in (7)–(9) is similar to that in (3), all the corresponding parameters can be taken into the expression regularly.

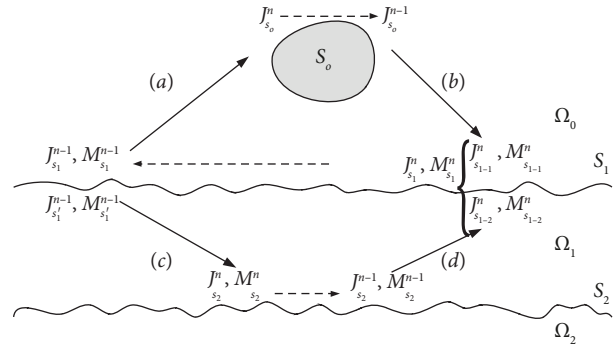

Figure 2: The mutual coupling strategy among the boundaries.

However, the local incident angle is determined by the local incident wave and normal vectors on the boundaries. The local incident wave vectors are the directions from the source point to the field point, and they replace $\hat{\mathbf{k}}_i$ in (3). $\hat{\mathbf{n}}_2$ is the surface normal vector to S_2, $\hat{\mathbf{n}}_1'$ is the lower surface normal vector to S_1. $\mathbf{L}_1$, $\mathbf{K}_1$, $\mathbf{L}_2$, and $\mathbf{K}_2$ are linear operators, and they can be found in [12].

2.3. Far Zone Scattering of the Composite Model. The total equivalent currents on the surfaces in Ω_0 can be expressed as follows:

$$\mathbf{J}_{s_o}(\mathbf{r}) = \mathbf{J}_{s_o}^{1}(\mathbf{r}) + \mathbf{J}_{s_o}^{2}(\mathbf{r}) + \cdots + \mathbf{J}_{s_o}^{n}(\mathbf{r})(\mathbf{r} \in S_o), \tag{10}$$

$$\mathbf{J}_{s_1}(\mathbf{r}) = \mathbf{J}_{s_1}^{1}(\mathbf{r}) + \mathbf{J}_{s_1}^{2}(\mathbf{r}) + \cdots + \mathbf{J}_{s_1}^{n}(\mathbf{r})(\mathbf{r} \in S_1), \tag{11a}$$

$$\mathbf{M}_{s_1}(\mathbf{r}) = \mathbf{M}_{s_1}^{1}(\mathbf{r}) + \mathbf{M}_{s_1}^{2}(\mathbf{r}) + \cdots + \mathbf{M}_{s_1}^{n}(\mathbf{r})(\mathbf{r} \in S_1). \tag{11b}$$

In our simulations, an error function v of the object is chosen as a rule to control the convergence in this model. The iteration begins with the first-order currents $\mathbf{J}_{s_o}^{1}(\mathbf{r})$, and terminates with $\mathbf{J}_{s_o}(\mathbf{r})$ reaching stable. The error function [20] is defined as follows:

$$v = \frac{\left|\mathbf{J}_{s_o}^{n}(\mathbf{r})\right|}{\left|\sum_{m=1}^{n} \mathbf{J}_{s_o}^{m}(\mathbf{r})\right|}, \tag{12}$$

where the notation of $|\cdot|$ indicates the Euclidean 2-norm of a vector. When $v < 0.001$, the interaction process is assumed to be stable and will stop. Then, the far zone fields $\mathbf{E}_{s_o}$ and $\mathbf{E}_{s_1}$ in Ω_0 can be calculated through the stable currents on the object and the upper layer rough surface by using Huygens's principle. The NRCS [19] can be calculated by

$$\sigma(\theta_s) = \lim_{r \longrightarrow \infty} \frac{2\pi r\left|\mathbf{E}_{s1}(\theta_s) + \mathbf{E}_o(\theta_s)\right|^2}{P_{\text{inc}}}. \tag{13}$$

P_{inc} is the power impinging upon the composite model, and it can be found in [21]. The process of vertical (VV) polarization is analogous to that of HH polarization, and the incident wave $\mathbf{H}^{\text{inc}}(\mathbf{r}) = \hat{\mathbf{y}}\phi^{\text{inc}}(\mathbf{r})$. It will be omitted in this paper.

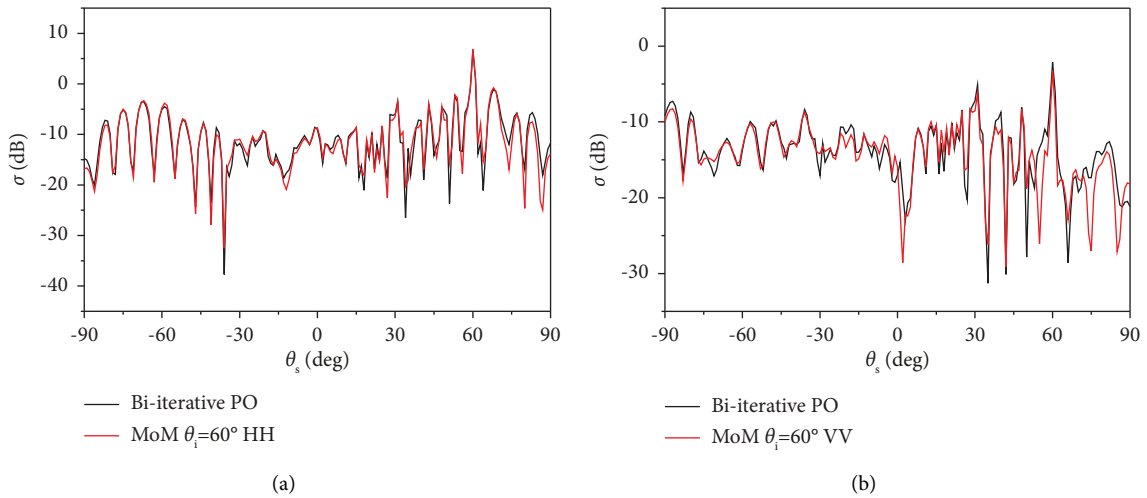

Figure 3: Comparison of NRCS from a cylinder above two-layered soil surfaces using the bi-iterative PO and MOM with (a) HH and (b) VV polarizations.

3. Results and Discussion

In this section, the NRCS of the composite model from a 2D PEC object and 1D underlying two-layered soil surfaces is calculated and analyzed for HH and VV polarizations. The numerical results are averaged by 30 Monte Carlo realizations unless noted otherwise.

Scattering from a PEC cylinder and two-layered soil surfaces calculated by the bi-iterative PO method for one composite realization is shown in Figure 3. The numerical results by the MoM [22] are presented to validate our code. The incident frequency is $f = 0.435$ GHz, the incident angle is $\theta_i = 60°$, the length of soil surface is $L = 102.4\lambda$, and the tapering parameter is $g = L/4$. The root mean square (RMS) height and correlation length for the upper and lower surfaces are $\delta_1 = 0.1\lambda, l_1 = 1.0\lambda, \delta_2 = 0.2\lambda$, and $l_2 = 1.5\lambda$. The cylinder radius is $r = 2\lambda$. Other parameters are $d = 4\lambda$ and $h = 4\lambda$. The soil moisture values are $m_{v1} = 0.08\text{cm}^3/\text{cm}^3$ and $m_{v2} = 0.12\text{cm}^3/\text{cm}^3$ for the upper and lower layers, and the corresponding relative permittivities are $\varepsilon_{r1} = (8.2, 1.2)$ and $\varepsilon_{r2} = (11.1, 1.4)$. The soil mixture model is the one by Peplinski et al. [15, 23]. As shown in Figure 3, the results by the two different methods match very well for most observation angles under different polarizations.

The computational time and memory requirement of the two methods for one composite realization of Figure 3 are shown in Table 1. The memory by our method is only 0.028% of that by MOM. The computational times are approximately 9.81%–19.6% of those by MoM for HH and VV polarizations. This finding illustrates that our method remarkably saves computer resources. All simulations are obtained on a computer with a 2.33 GHz processor (Intel (R) Core(TM)2 Quad CPU Q8200), 3.5 GB memory, and Visual Fortran 6.5 compiler.

To further show the validity of our method, the D-RCS [24] from a cylinder above two-layered soil surfaces that is the same model as in Figure 3 is calculated by our method and is compared with MoM for one realization in Figure 4.

Table 1: CPU time and required memory in Figure 3.

Polarization	Method	Memory (MB)	Time (s)
HH	MOM	2693.93	214
	Bi-iterative PO	0.75	21
VV	MOM	2693.93	107
	Bi-iterative PO	0.75	21

As shown in Figure 4, the results by the two different methods match very well for most observation angles under different polarizations.

The dependence of the roughness of Gaussian rough surface on NRCS analyzed with HH polarizations is shown in Figure 5. When the soil moistures are set as $m_{v1} = 0.12\text{cm}^3/\text{cm}^3$, and $m_{v2} = 0.25\text{cm}^3/\text{cm}^3$ for the upper and lower layer surfaces, and the corresponding relative permittivities are $\varepsilon_{r1} = (11.1, 1.4)$ and $\varepsilon_{r2} = (21.6, 2.1)$ at f = 0.435GHz. $\theta_i = 20°$, the other parameters are the same as those in Figure 3. Figure 5(a) shows the comparison for a fixed correlation length of $l_1 = l_2 = 1.0\lambda$ and a varying RMS height $\delta_1 = \delta_2$ for both surfaces. An obvious peak appears in the specular direction for $\delta_1 = \delta_2 = 0.01\lambda$, and the specular peak decreases with the increase in RMS height. The reason is that the rough surfaces become rough and the incoherent scattering becomes strong. Figure 5(b) shows the comparison for a fixed RMS height of $\delta_1 = \delta_2 = 0.2\lambda$ and a varying correlation length $l_1 = l_2$ for both surfaces. The rough surface becomes smooth with the increase in the correlation length. As a result, a large amount of energy will be concentrated in the specular directions.

The backscattering for different soil moisture contents of the upper layer from the rough surface and composite models with VV polarization is shown in Figure 6. f = 0.435GHz and m_{v1} are set as 0.08, 0.12, and $0.2\text{cm}^3/\text{cm}^3$ for the upper layer, and the corresponding relative permittivities are $\varepsilon_{r1} = (8.2, 1.2)$, $(11.1, 1.4)$, and $(17.4, 2.1)$. The lower layer soil moisture m_{v2} is fixed to $0.25\text{cm}^3/\text{cm}^3$ with the relative permittivity $\varepsilon_{r2} = (21.6, 2.1)$. The

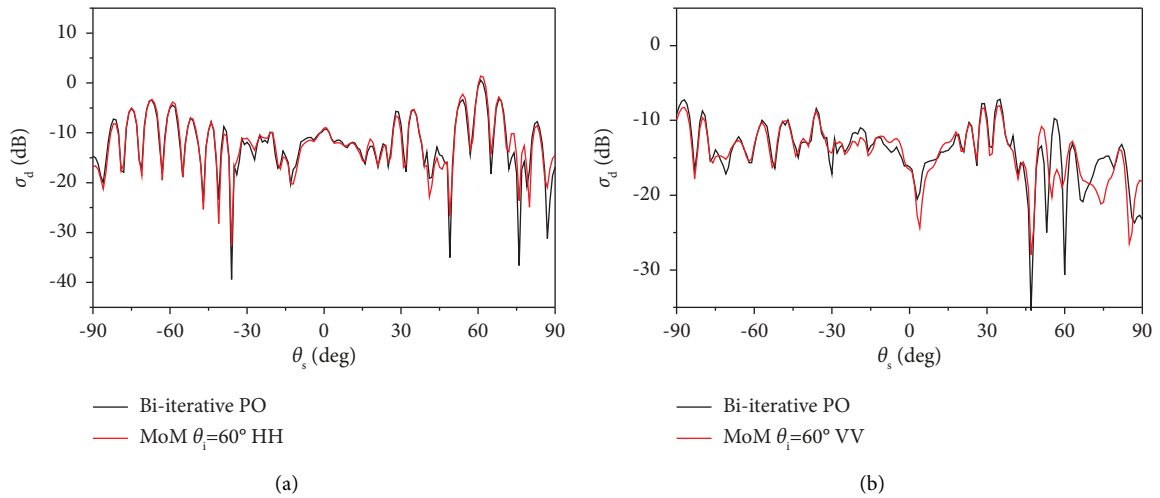

FIGURE 4: The comparison of D-RCS from a cylinder above two-layered soil surfaces using the bi-iterative PO and MOM with (a) HH and (b) VV polarizations.

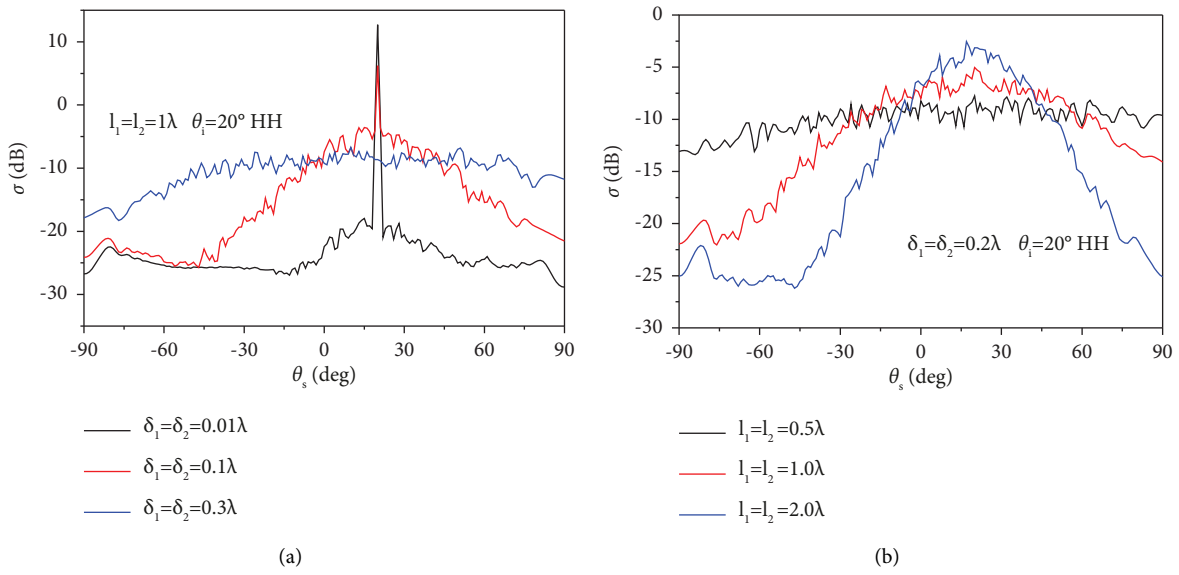

FIGURE 5: Angular distribution of NRCS for different roughness, (a) different δ, and (b) different l.

backscattered field decreases approximately linear with the increase in the incident angle for the two-layered soil surface. However, the backscattering field oscillates with the increase in the incident angle for the composite model. This result is attributed to the multipath effect between the object and the underlying rough surface. In addition, the scattering field is increased in nearly all the observation angles with the increase in soil moisture because of the decrease in the loss tangent of the upper layer soil.

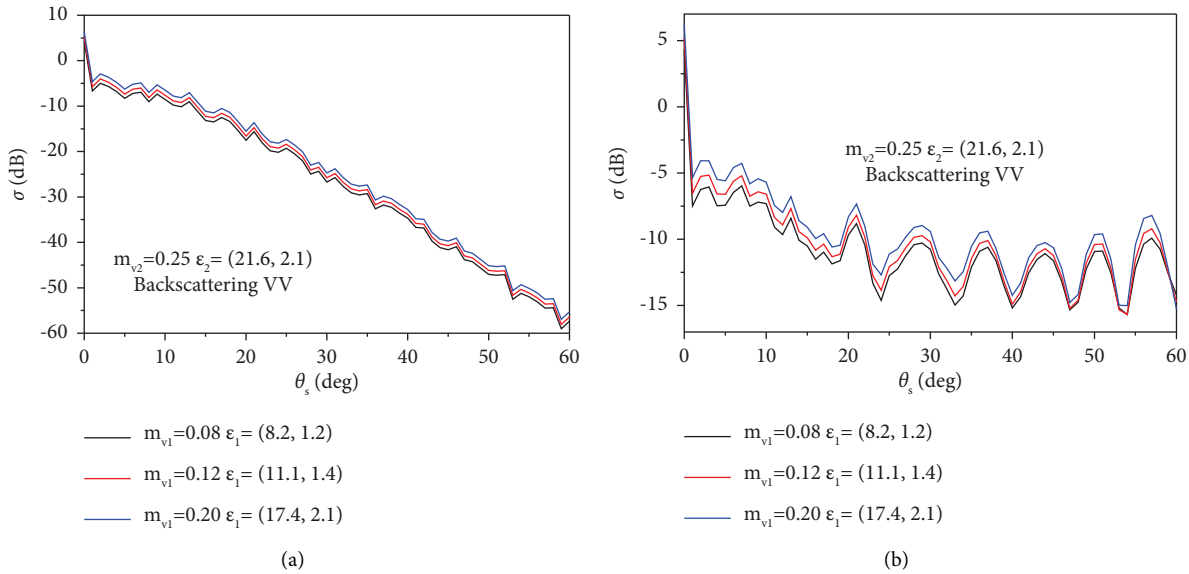

FIGURE 6: Backscattering for different soil moisture contents of the upper layer for (a) two-layered soil surfaces and (b) the composite model.

4. Conclusions

The composite scattering from a PEC object above a two-layered rough soil surface is investigated in this study. A bi-iterative PO method is used to deal with the problem. The NRCS of the composite model is validated by comparing with that from the conventional MoM. The comparison results show the validity of the adopted method. The comparison of computer resources also shows the efficiency of our method. The simulated results show that the coupling effect is remarkable in the composite model, and the soil moisture of the upper surface affects the NRCS considerably. This study can provide a fast and efficient theoretical reference for target detection above the soil and radar remote sensing retrieval of the soil moisture.

In our future study, the complex 3D model of an object and layered rough surfaces will be considered for practical applications.

Data Availability

Data sharing is not applicable to this article as no new data were created or analyzed in this study.

Conflicts of Interest

The authors declare that they have no conflicts of interest.

Acknowledgments

This work was supported by the National Natural Science Foundation of China (Grant nos. 62201435, 61871457, 61971338, and U21A20457) and the Foundation for Innovative Research Groups of the National Natural Science Foundation of China (Grant no. 61621005).

References

[1] W. A. Cumming, "The dielectric properties of ice and snow at 3.2 centimeters," *Journal of Applied Physics*, vol. 23, no. 7, pp. 768–773, 1952.

[2] A. Spizzichino, *The Scattering of Electromagnetic Waves from Rough Surfaces*, Pergamon Press, Oxford, England, 1963.

[3] M. E. Brown, D. Entekhabi, E. Njoku, and P. O'Neill, "The soil moisture active and passive mission (SMAP)," *Proceedings of the IEEE*, vol. 98, 2010.

[4] Y. H. Kerr, P. Waldteufel, J. P. Wigneron et al., "The SMOS mission: new tool for monitoring key elements ofthe global water cycle," *Proceedings of the IEEE*, vol. 98, no. 5, pp. 666–687, 2010.

[5] F. Mahini and H. Ashrafiuon, "Autonomous surface vessel target tracking experiments in simulated rough sea conditions," in *Proceedings of the ASME 2012 Dynamic Systems and Control Conference Joint with the Jsme 2012 Motion and Vibration Conference*, Florida, FL, USA, October 2012.

[6] H. X. Ye and Y. Q. Jin, "Fast iterative approach to difference scattering from the target above a rough surface," *IEEE Transactions on Geoscience and Remote Sensing*, vol. 44, no. 1, pp. 108–115, 2006.

[7] J. Li, L. X. Guo, Y. C. Jiao, and K. Li, "Investigation on wideband scattering of a 2-D target above 1-D randomly rough surface by FDTD method," *Optics Express*, vol. 19, no. 2, pp. 1091–1100, 2011.

[8] L. X. Guo and R. W. Xu, "An efficient multiregion FEM-BIM for composite scattering from an arbitrary dielectric target above dielectric rough sea surfaces," *IEEE Transactions on Geoscience and Remote Sensing*, vol. 53, no. 7, pp. 3885–3896, 2015.

[9] H. X. Ye and Y. Q. Jin, "A hybrid analytic-numerical algorithm of scattering from an object above a rough surface," *IEEE Transactions on Geoscience and Remote Sensing*, vol. 45, no. 5, pp. 1174–1180, 2007.

[10] J. Li, L. X. Guo, and Q. He, "Hybrid FE-BI-KA method in analysing scattering from dielectric object above sea surface," *Electronics Letters*, vol. 47, no. 20, pp. 1147-1148, 2011.

[11] J. Li, L. X. Guo, S. R. Chai, and Y. C. Jiao, "Electromagnetic scattering from a PEC object above a dielectric rough sea surface by a hybrid PO–PO method," *Waves in Random and Complex Media*, vol. 25, no. 1, pp. 60–74, 2015.

[12] J. Li, K. Li, L. X. Guo, and Z. L. Ren, "A Bi-iterative model for electromagnetic scattering from a PEC object partially buried in rough sea surface," *IEEE Geoscience and Remote Sensing Letters*, vol. 15, no. 4, pp. 493–497, 2018.

[13] R. Wang, L. Guo, and Z. B. Zhang, "Scattering from contaminated rough sea surface by iterative physical optics model," *IEEE Geoscience and Remote Sensing Letters*, vol. 13, no. 4, pp. 500–504, 2016.

[14] K. Li, L. X. Guo, and J. Li, "Three dimensional electromagnetic scattering of two-layer rough surfaces using physical optics approximation algorithm," *Progress In Electromagnetics Research M*, vol. 74, pp. 159–168, 2018.

[15] A. Tabatabaeenejad, X. Duan, and M. Moghaddam, "Coherent scattering of electromagnetic waves from two-layer rough surfaces within the Kirchhoff regime," *IEEE Transactions on Geoscience and Remote Sensing*, vol. 51, no. 7, pp. 3943–3953, 2013.

[16] M. El-Shenawee, "Polarimetric scattering from two-layered two-dimensional random rough surfaces with and without buried objects," *IEEE Transactions on Geoscience and Remote Sensing*, vol. 42, no. 1, pp. 67–76, 2004.

[17] A. Q. Wang, L. X. Guo, and C. Chai, "Fast numerical method for electromagnetic scattering from an object above a large-scale layered rough surface at large incident angle: vertical polarization," *Applied Optics*, vol. 50, no. 4, pp. 500–508, 2011.

[18] J. Li, L. X. Guo, and H. Zeng, "FDTD Investigation on bistatic scattering from a target above two-layered rough surfaces using upml absorbing condition," *Progress In Electromagnetics Research*, vol. 88, pp. 197–211, 2008.

[19] E. I. Thorsos, "The validity of the Kirchhoff approximation for rough surface scattering using a Gaussian roughness spectrum," *Journal of the Acoustical Society of America*, vol. 83, no. 1, pp. 78–92, 1988.

[20] W. Yang, Z. Zhao, C. Qi, W. Liu, and Z. P. Nie, "Iterative hybrid method for electromagnetic scattering from a 3-D object above a 2-D random dielectric rough surface," *Progress In Electromagnetics Research*, vol. 117, pp. 435–448, 2011.

[21] L. Tsang, J. A. Kong, and K. H. Ding, *Scattering of Electromagnetic Waves, Numerical Simulations*, Wiley-Interscience, New York, NY, USA, 2001.

[22] A. Q. Wang, L. X. Guo, and C. Chai, "Electromagnetic scattering from two-layered rough interfaces with a PEC object:vertical polarization," *Chinese Physics B*, vol. 20, no. 5, Article ID 050202, 2011.

[23] N. R. Peplinski, F. T. Ulaby, and M. C. Dobson, "Dielectric properties of soils in the 0.3-1.3-GHz range," *IEEE Transactions on Geoscience and Remote Sensing*, vol. 33, no. 3, pp. 803–807, 1995.

[24] J. T. Johnson, "A numerical study of scattering from an object above a rough surface," *IEEE Transactions on Antennas and Propagation*, vol. 50, no. 10, pp. 1361–1367, 2002.